Research Square

Preprints are preliminary reports that have not undergone peer review.
They should not be considered conclusive, used to inform clinical practice,
or referenced by the media as validated information.

Hippocampal CA1 TOM70 Overexpression Attenuates Type 2 Diabetes-Associated Cognitive Impairment and Enhances Mitochondrial Quality Control in Mice

Wei Zhang
Zhongnan Hospital of Wuhan University
Jinying Zhao
Zhongnan Hospital of Wuhan University
Xuerui Xiang
Zhongnan Hospital of Wuhan University
Yuliang Zhou
Zhongnan Hospital of Wuhan University
Shi Cheng
Zhongnan Hospital of Wuhan University
Zhipeng Xu
xzhp14@sina.com
Zhongnan Hospital of Wuhan University

Research Article

Keywords: Type 2 diabetes mellitus, TOM70, Mitophagy, Hippocampus, Recognition memory, Mitochondrial oxidative stress

Posted Date: November 12th, 2026

DOI: https://doi.org/10.21203/rs.3.rs-11539379/v1

License: This work is licensed under a Creative Commons Attribution 4.0 International License.
Read Full License

Additional Declarations: No competing interests reported.

Abstract

Type 2 diabetes mellitus (T2DM) is associated with cognitive impairment, in which mitochondrial dysfunction and impaired mitochondrial quality control are increasingly implicated. The translocase of the outer mitochondrial membrane 70 (TOM70) serves as a receptor for PINK1 import, a key upstream event in PINK1/Parkin-mediated mitophagy; however, its role in T2DM-associated cognitive decline remains unclear. Here, we overexpressed TOM70 in the hippocampal CA1 region of high-fat diet/streptozotocin-induced T2DM mice via adeno-associated virus (AAV9-hSyn) and assessed recognition memory (novel object recognition test, NORT), locomotor activity and immobility (open field test, OFT), mitochondrial ultrastructure (transmission electron microscopy), mitophagy-related proteins (LC3-I/II, p62, TOMM20, p-Ser65-Ub; Western blotting), mitochondrial superoxide (MitoSOX), and dendritic spine density (Golgi staining). TOM70 overexpression restored the NORT discrimination index and reduced immobility time in T2DM mice, preserved mitochondrial cristae architecture, increased LC3-II and p-Ser65-Ub while decreasing p62, lowered mitochondrial superoxide in CA1, CA3, and DG, and increased spine density in CA1 and CA3. The LC3-II/LC3-I ratio and TOMM20 levels did not change significantly, and PINK1 stabilization, Parkin translocation, and autophagic flux were not directly measured. These findings suggest that CA1-specific TOM70 overexpression attenuates recognition-memory deficits in T2DM mice, with molecular changes consistent with enhanced PINK1/Parkin-associated mitophagy, reduced oxidative stress, and preserved synapses, supporting TOM70 as a candidate target for further study in T2DM-associated cognitive impairment.

Introduction

Type 2 diabetes mellitus (T2DM) accounts for more than 90% of all diabetes cases and represents a major global health burden [1]. Cognitive impairment has emerged as a frequent and debilitating central nervous system complication of T2DM, substantially compromising patients' quality of life [2]. Epidemiological evidence indicates that individuals with T2DM have an approximately 1.5-fold increased risk of developing Alzheimer's disease (AD) [3], establishing T2DM as a significant modifiable risk factor for dementia.

The pathogenesis of T2DM-associated cognitive impairment (T2DM-CI) is multifactorial and involves chronic hyperglycemia, central insulin resistance, cerebrovascular dysfunction, and neuroinflammation [4]. Central insulin resistance leads to excessive insulin-mediated sequestration of insulin-degrading enzyme (IDE), thereby impairing amyloid-β (Aβ) clearance and promoting Aβ aggregation [4, 5]. Concurrently, Aβ competitively binds to insulin receptors, disrupting the PI3K-Akt signaling pathway and enhancing glycogen synthase kinase 3β (GSK-3β) activity, which accelerates Tau hyperphosphorylation [6]. Among these interconnected pathological mechanisms, mitochondrial dysfunction is increasingly recognized as a key mediator [7].

Postmortem analyses of AD brains have revealed markedly impaired mitophagy in the hippocampus; quantitative studies have demonstrated significantly higher mitochondrial numbers in AD hippocampi

than in healthy controls, indicating defective clearance of damaged mitochondria [8]. In streptozotocin (STZ)-induced sporadic AD models, all hippocampal subregions (CA1, CA2, CA3, and DG) exhibited significant volumetric reductions, with CA1 showing the most severe mitochondrial functional impairment, suggesting that subregion-specific mitochondrial dysfunction contributes to neuronal death [9].

The translocase of the outer mitochondrial membrane 70 (TOM70) is a critical component of the mitochondrial protein import system. TOM70 functions as an essential receptor for the mitochondrial translocation of PTEN-induced kinase 1 (PINK1), a master regulator of mitophagy [10]. Under physiological conditions, PINK1 is imported into healthy mitochondria via the TOM70-TIM23 complex and rapidly degraded therein. Upon mitochondrial damage and dissipation of the membrane potential, PINK1 import is impaired, leading to its stabilization on the outer mitochondrial membrane [11], where it phosphorylates ubiquitin at serine 65 (p-Ser65-Ub). Phosphorylated ubiquitin recruits and activates the E3 ubiquitin ligase Parkin, which in turn ubiquitinates outer mitochondrial membrane proteins, tagging damaged mitochondria for autophagic engulfment and lysosomal degradation, a process accompanied by the degradation of the selective autophagy receptor p62/SQSTM1 [12, 13].

Decreased TOM70 expression has been documented in the brain tissues of AD patients [14]. Furthermore, Aβ peptides (Aβ1–40 and Aβ1–42) have been shown to enter mitochondria through the TOM/TIM complex [15], suggesting that TOM70 dysfunction may exacerbate both impaired mitophagy and mitochondrial Aβ accumulation. Importantly, because TOM70 is essential for PINK1 mitochondrial import, its reduced expression or functional impairment prevents proper PINK1 localization to the outer mitochondrial membrane and consequently diminishes mitophagy [10].

Based on this evidence, we hypothesized that enhancing TOM70 expression in the hippocampus would promote PINK1/Parkin-mediated mitophagy, reflected by increased p-Ser65-Ub and decreased p62 levels, facilitating the clearance of damaged mitochondria and alleviating mitochondrial oxidative stress. In the present study, we investigated whether adeno-associated virus (AAV)-mediated TOM70 overexpression in the hippocampal CA1 region protects against cognitive decline, mitochondrial structural damage, and oxidative stress in a T2DM mouse model, and sought to elucidate the molecular mechanisms underlying PINK1/Parkin-mediated mitophagy activation.

Materials and Methods

Animals

Adult male C57BL/6J mice (aged 8 weeks) were obtained from Shulaibao (Wuhan) Biotechnology Co., Ltd. The mice were group-housed (four per cage) under controlled environmental conditions (temperature, 22 ± 2°C; humidity, 50–60%; 12 h/12 h light-dark cycle, lights on at 07:00) with ad libitum access to standard chow and water, and were allowed to acclimate for one week. All animal experiments were approved by the Institutional Animal Care and Use Committee of Zhongnan Hospital of Wuhan

University (Approval No. ZN2026117) and conducted in strict accordance with the "Regulations for the Administration of Affairs Concerning Experimental Animals of China".

T2DM Mouse Model

To establish the T2DM model, mice were fed a high-fat diet (HFD; 20% protein, 20% carbohydrate, 60% fat) for 6 weeks, followed by intraperitoneal (i.p.) injections of streptozotocin (STZ; 40 mg/kg; dissolved in 0.1 mol/L sodium citrate-hydrochloric acid buffer, pH 4.5) for 3 consecutive days. Age-matched control mice were fed a normal diet (ND) and received an equal volume of citrate buffer on the same schedule. Fasting blood glucose (FBG) levels were measured in tail-vein blood samples (overnight fast) using a glucometer. The T2DM model was considered successfully established when FBG levels exceeded 11.1 mmol/L for at least one consecutive week [16, 17]. Body weight and FBG were monitored weekly throughout the experimental period. After successful model establishment, both T2DM mice and their age-matched controls were randomly subdivided into two groups, yielding four experimental groups (n = 10 per group): C57/AAV-ctrl, C57/AAV-TOM70(+), T2DM/AAV-ctrl, T2DM/AAV-TOM70(+).

AAV-Mediated TOM70 Overexpression in Hippocampal CA1

The recombinant adeno-associated viral vectors rAAV9-hSyn-Tomm70a-2A-EGFP-WPRE-hGH polyA (AAV-TOM70) (5.0×10^{12} vg/mL) and the empty control vector rAAV9-hSyn-2A-EGFP-WPRE-hGH polyA (AAV-ctrl) (5.0×10^{12} vg/mL) were obtained from Wuhan Shumi Brain Science and Technology Co., Ltd. (Wuhan, China). After successful T2DM model establishment, mice underwent bilateral stereotaxic injection of AAV into the hippocampal CA1 region. Briefly, mice were anesthetized with sodium pentobarbital (1% solution, 50 mg/kg, i.p.) and secured in a stereotaxic frame (RWD Life Science, Shenzhen, China). A midline scalp incision was made, and bilateral burr holes were drilled at the following coordinates relative to bregma: anteroposterior (AP) = -2.0 mm, mediolateral (ML) = ± 1.45 mm. Using a 10 μL NanoFil syringe fitted with a 35-gauge needle, 500 nL of AAV-TOM70 or AAV-ctrl was infused bilaterally into the CA1 (dorsoventral, DV = -1.4 mm) [18] at a rate of 50 nL/min via a syringe pump. After infusion, the needle was left in place for 10 min and then slowly withdrawn over 5 min to minimize backflow. The incision was closed with surgical sutures. Behavioral tests were initiated 4 weeks after viral injection to allow optimal transgene expression.

Behavioral Testing

Behavioral testing was conducted during the light phase (09:00–15:00) in a sound-attenuated room maintained at 22 ± 2°C and 50–60% humidity. Before testing, mice were handled daily for 5 min over 3 consecutive days to habituate them to the experimenter. The open field test (OFT) and the novel object recognition test (NORT) were performed sequentially at 24-h intervals, and all recordings were analyzed by investigators blinded to group allocation. In the OFT, spontaneous locomotor activity and anxiety-like behaviors were assessed by placing each mouse in the center of a 50 × 50 × 40 cm arena and allowing

free exploration for 5 min; total distance traveled and immobility time were quantified using a video-tracking system. Recognition memory was evaluated using the NORT, which comprised a 10-min habituation session in an empty arena, a 10-min training session with two identical objects, and a 5-min test session in which one familiar object was replaced by a novel object of a different shape, color, and texture. The discrimination index (DI) was calculated as [(time exploring the novel object - time exploring the familiar object) / (time exploring the novel object + time exploring the familiar object)] × 100%. Between sessions, the arena and objects were thoroughly cleaned with 75% ethanol to eliminate residual olfactory cues.

MitoSOX Red Staining and Immunofluorescence

Mice were deeply anesthetized with sodium pentobarbital (50 mg/kg, i.p.) and transcardially perfused with ice-cold phosphate-buffered saline (PBS) to clear the cerebral vasculature. Brains were rapidly removed, embedded in OCT compound, and frozen at -80°C. Fresh coronal cryostat sections (20 μm thick) were cut on a cryostat (Leica CM3050S, Wetzlar, Germany) and mounted onto gelatin-coated glass slides. For MitoSOX staining, fresh sections were incubated with MitoSOX Red mitochondrial superoxide indicator working solution (5 μmol/L; Invitrogen, M36008) in a humidified chamber at 37°C for 30 min in the dark. After incubation, sections were gently washed three times (5 min each) with pre-warmed HBSS (37°C). Sections were then fixed with 4% paraformaldehyde (PFA) at room temperature for 10 min, permeabilized with 0.3% Triton X-100 in PBS for 15 min, and blocked with 3% bovine serum albumin (BSA) and 2% normal goat serum in PBS at room temperature for 1 h. Sections were incubated with rabbit anti-NeuN primary antibody (1:200; Abcam, ab177487) diluted in 1% BSA in PBS overnight at 4°C in a humidified chamber. After three PBS washes, sections were incubated with Alexa Fluor 488-conjugated goat anti-rabbit IgG secondary antibody (1:500; Invitrogen, A-11008) for 2 h at room temperature in the dark. After three additional PBS washes, sections were mounted with ProLong Diamond Antifade Mountant containing DAPI (1 μg/mL; Invitrogen, P36962) and coverslipped. Images were acquired using a fluorescence microscope (Olympus BX53F, Tokyo, Japan). The mean MitoSOX fluorescence intensity within $NeuN^+/DAPI^+$ neurons in the hippocampal CA1 region was quantified using ImageJ (NIH, Bethesda, MD, USA). Negative controls omitting the primary antibodies were included in all experiments. For each sample, at least 12 sections were analyzed, and values were averaged across three biological replicates per group; all analyses were performed by an investigator blinded to group allocation.

Western Blotting

Hippocampal tissues were homogenized in ice-cold RIPA buffer (10 mmol/L Tris-Cl, 150 mmol/L NaCl, 1% NP-40, 0.5% sodium deoxycholate, 0.1% SDS; pH 7.4) supplemented with protease and phosphatase inhibitors (Roche). Lysates were centrifuged at 12,000 × g for 10 min at 4°C, and protein concentrations were determined using a BCA assay (Thermo Fisher Scientific). Equal amounts of protein (30 μg per lane) were separated by 10% SDS-PAGE and wet-transferred (100 V, 60 min, 4°C) onto 0.45 μm

nitrocellulose membranes (Millipore). Membranes were blocked with 5% nonfat milk in TBST for 1 h and then incubated overnight at 4°C with the following primary antibodies: rabbit anti-TOM70 (1:1000; CST, #49360), rabbit anti-LC3A/B (1:1000; CST, #12741), and mouse anti-β-actin (1:10000; Proteintech, 66009-1-Ig). After TBST washes, membranes were incubated with HRP-conjugated secondary antibodies (goat anti-rabbit, 1:5000; CST, #7074; horse anti-mouse, 1:5000; CST, #7076) for 1 h at room temperature. Bands were visualized using SuperSignal West Pico PLUS substrate (Thermo Fisher Scientific) and imaged on a ChemiDoc XRS+ system (Bio-Rad). Densitometric analysis was performed using ImageJ with β-actin as the loading control. For reprobing, membranes were stripped with Restore buffer (Thermo Fisher Scientific), re-blocked, and re-probed. All experiments were repeated independently at least three times.

Golgi Staining and Dendritic Spine Analysis

Golgi staining was performed using the Hito Golgi Box OptimStain PreKit (Hitobiotec Corp., USA). Mice were anesthetized with sodium pentobarbital (50 mg/kg, i.p.) and decapitated, and the brains were rapidly removed. Brains were immersed in impregnation solution (solution A:solution B = 1:1) at room temperature in the dark for 14 days, followed by incubation in solution C at 4°C for 2 days. Coronal sections (100 μm thick) were cut on a vibratome (Leica VT1000S), mounted onto gelatin-coated glass slides, and processed for staining and coverslipping according to the manufacturer's protocol. Images were acquired using an Olympus BX53F microscope. Dendritic spine density was quantified on secondary and tertiary branches of hippocampal CA1 pyramidal neurons using ImageJ and expressed as the number of spines per 10 μm of dendritic length.

Transmission Electron Microscopy

Hippocampal CA1 tissues were cut into approximately 1 mm^3 blocks, fixed in 2.5% glutaraldehyde at 4°C for 4 h, and rinsed with PBS. After post-fixation with 1% osmium tetroxide and en bloc staining with 2% uranyl acetate, samples were dehydrated through a graded acetone series and embedded in epoxy resin. Ultrathin sections (60 nm thick) were cut on an ultramicrotome (Leica EM UC7) and counterstained with lead citrate. Ultrastructural observations were performed using a transmission electron microscope (Thermo Fisher Scientific, USA). Mitochondrial morphology was assessed by two independent investigators blinded to group assignment.

Statistical Analysis

All statistical analyses were performed using IBM SPSS Statistics 26.0 and GraphPad Prism 10.0. Data are presented as mean ± standard error of the mean (SEM). The Shapiro-Wilk test was used to assess the normality of data distribution. Because all data in this study were normally distributed, group comparisons were performed using one-way analysis of variance (ANOVA) followed by Tukey's post hoc

test for multiple comparisons. A two-tailed P value < 0.05 was considered statistically significant. All experiments were performed with a minimum of three independent biological replicates.

Results

Establishment of the T2DM Model and Validation of TOM70 Overexpression

To evaluate the stability of the T2DM model, body weight and FBG levels were monitored throughout the study. Compared with the control group, FBG levels in T2DM mice remained consistently above 11.1 mmol/L from week 8 onward (i.e., one week after completion of STZ injections at week 7; $P < 0.001$), confirming successful establishment of the T2DM model. The detailed experimental flow chart for this study is shown in Fig. 1. Bilateral stereotaxic injection of AAV-TOM70 into the hippocampal CA1 region significantly increased TOM70 protein expression in both control and T2DM mice compared with their respective AAV-ctrl-injected controls, as confirmed by Western blot analysis ($P < 0.05$; Fig. 2A-B). These results validate the efficient and targeted overexpression of TOM70 in the hippocampal CA1 subregion.

TOM70 Overexpression Ameliorates Behavioral Deficits in T2DM Mice

In the open field test, C57/AAV-TOM70(+) mice traveled a significantly greater total distance than C57/AAV-ctrl mice ($P < 0.05$; Fig. 3A). No significant differences in center zone time were observed across groups (ns; Fig. 3B). T2DM/AAV-TOM70(+) mice exhibited significantly reduced immobility time compared with T2DM/AAV-ctrl mice ($P < 0.01$; Fig. 3C). In the novel object recognition test (NORT), T2DM/AAV-ctrl mice showed a significantly lower discrimination index (DI) compared with C57/AAV-ctrl mice ($P < 0.05$; Fig. 3E). TOM70 overexpression significantly increased the DI in T2DM/AAV-TOM70(+) mice ($P < 0.05$ vs. T2DM/AAV-ctrl; Fig. 3E), restoring novel object preference to levels comparable to those of controls. TOM70 overexpression also prolonged the time spent exploring the novel object in both control and T2DM mice ($P < 0.05$; Fig. 3D).

TOM70 Overexpression Restores Mitochondrial Ultrastructure in the Hippocampal CA1 Region

Transmission electron microscopy (TEM) was used to examine mitochondrial ultrastructure in the hippocampal CA1 region across all experimental groups (Fig. 4). In C57/AAV-ctrl mice, mitochondria exhibited a typical elongated oval morphology, with densely packed, well-organized cristae showing clear lamellar structure and intact, continuous outer and inner membranes (Fig. 4A). C57/AAV-TOM70(+) mice showed preserved mitochondrial morphology with no apparent structural abnormalities (Fig. 4B). In contrast, T2DM/AAV-ctrl mice displayed mitochondrial structural damage characterized by: (i) marked mitochondrial swelling with reduced matrix electron density and translucent vacuolar changes; (ii)

variable degrees of cristae disruption, ranging from partial loss of lamellar organization to complete cristae disintegration; and (iii) focal discontinuities in the outer and/or inner mitochondrial membranes, with some mitochondria exhibiting extensive vacuolization (Fig. 4C). TOM70 overexpression in T2DM mice (T2DM/AAV-TOM70(+)) improved mitochondrial morphology: the lamellar architecture of the cristae was largely restored, with parallel arrays of folded cristae membranes clearly visible and improved outer and inner membrane continuity, although occasional mild swelling was still observed (Fig. 4D).

Effect of TOM70 Overexpression on Hippocampal LC3 and Mitophagy-Related Protein Expression

Western blot analysis was performed to evaluate the effect of TOM70 overexpression on the autophagy-related microtubule-associated protein light chain 3 (LC3) pathway and mitophagy-related proteins in the hippocampus (Fig. 5). Densitometric quantification revealed that TOM70 overexpression significantly increased LC3-II protein levels in both C57/AAV-TOM70(+) and T2DM/AAV-TOM70(+) mice compared with their respective AAV-ctrl controls ($P < 0.01$; Fig. 5C). LC3-I expression was also increased in both AAV-TOM70-treated groups ($P < 0.05$ in C57/AAV-TOM70(+); $P < 0.01$ in T2DM mice vs. T2DM/AAV-ctrl; Fig. 5B). The LC3-II/LC3-I ratio did not differ significantly among the experimental groups (ns; $P > 0.05$; Fig. 5D).

Among the mitophagy-related proteins, T2DM/AAV-ctrl mice exhibited significantly higher p62 protein levels than C57/AAV-ctrl mice ($P < 0.001$; Fig. 5E, F), and TOM70 overexpression significantly reduced p62 levels in T2DM/AAV-TOM70(+) mice compared with T2DM/AAV-ctrl mice ($P < 0.001$; Fig. 5F). In contrast, TOMM20 protein levels did not differ significantly among the four groups (ns; $P > 0.05$; Fig. 5G). Notably, p-Ser65-Ub levels were significantly lower in T2DM/AAV-ctrl mice than in C57/AAV-ctrl mice ($P < 0.01$; Fig. 5H), and TOM70 overexpression significantly increased p-Ser65-Ub levels in T2DM/AAV-TOM70(+) mice compared with T2DM/AAV-ctrl mice ($P < 0.001$; Fig. 5H). No significant differences in p62, TOMM20, or p-Ser65-Ub were observed between C57/AAV-ctrl and C57/AAV-TOM70(+) mice (ns; $P > 0.05$; Fig. 5F-H).

Effect of TOM70 Overexpression on Hippocampal Mitochondrial ROS Levels

To evaluate the effect of TOM70 overexpression on mitochondrial reactive oxygen species (ROS) levels in hippocampal neurons, MitoSOX Red staining was performed on fresh frozen brain sections, combined with NeuN immunofluorescence to identify mature neurons and DAPI for nuclear counterstaining (Fig. 6). Fluorescence microscopy revealed that MitoSOX fluorescence intensity was elevated in the CA1 region of T2DM/AAV-ctrl mice relative to C57/AAV-ctrl mice. Quantitative analysis of mean MitoSOX fluorescence within $NeuN^+/DAPI^+$ CA1 pyramidal neurons showed that TOM70 overexpression significantly reduced MitoSOX fluorescence intensity in the hippocampal CA1 region of T2DM/AAV-

TOM70(+) mice ($P < 0.01$; Fig. 7A). Similar trends were observed in the CA3 ($P < 0.01$; Fig. 7B) and DG ($P < 0.05$; Fig. 7C) subregions.

Effect of TOM70 Overexpression on Hippocampal Dendritic Spine Density

Golgi staining was used to assess the effects of TOM70 overexpression on dendritic spine density in hippocampal CA1 pyramidal neurons, CA3 pyramidal neurons, and DG granule cells (Fig. 8). No significant difference in spine density was observed between C57/AAV-ctrl and T2DM/AAV-ctrl mice in any of the three hippocampal subregions examined (ns, $P > 0.05$; Fig. 8A-C). TOM70 overexpression in T2DM mice (T2DM/AAV-TOM70(+)) significantly increased dendritic spine density in the CA1 (**$P < 0.01$; Fig. 8A) and CA3 ($P < 0.05$; Fig. 8B) subregions compared with T2DM/AAV-ctrl mice, whereas no significant change was detected in the DG (ns; Fig. 8C). In C57 mice, TOM70 overexpression did not significantly alter spine density in any of the subregions examined (ns vs. C57/AAV-ctrl; Fig. 8A-C).

Discussion

Summary of Main Findings

The present study demonstrates that hippocampal CA1-specific TOM70 overexpression confers neuroprotection against T2DM-associated cognitive impairment by preserving mitochondrial homeostasis and synaptic structural integrity. Our integrated behavioral, ultrastructural, molecular, and morphological analyses show that: (1) TOM70 overexpression significantly ameliorates T2DM-induced recognition memory deficits; (2) TOM70 restoration markedly improves mitochondrial ultrastructure, including recovery of cristae architecture and membrane integrity; (3) TOM70 upregulation increases LC3-II protein expression while decreasing p62 and increasing p-Ser65-Ub levels in the T2DM hippocampus, indicating enhanced PINK1/Parkin-mediated mitophagy, although the LC3-II/LC3-I ratio remained unchanged; (4) TOM70 overexpression reduces mitochondrial oxidative stress in hippocampal neurons; and (5) TOM70-mediated mitochondrial quality control protects dendritic spine density, the structural basis of synaptic plasticity, in the CA1 and CA3 hippocampal subregions under T2DM conditions. These findings establish TOM70 as a critical molecular link between mitochondrial protein import and cognitive health in T2DM.

TOM70, Mitophagy, and Mitochondrial Quality Control in T2DM

TOM70 is an essential receptor subunit of the translocase of the outer mitochondrial membrane (TOM) complex, which mediates the import of approximately 99% of nuclear-encoded mitochondrial proteins [19]. Beyond its canonical role as a protein import receptor, TOM70 also functions as an indispensable receptor for PINK1, the master initiator of mitophagy [10]. Under basal conditions, PINK1 is constitutively imported into healthy mitochondria through the TOM70-TIM23 pathway, where it is cleaved by the inner

membrane protease PARL and subsequently degraded by the ubiquitin-proteasome system [20]. Upon mitochondrial stress, such as membrane potential dissipation induced by chronic hyperglycemia, PINK1 import is blocked, leading to its accumulation on the outer mitochondrial membrane. Stabilized PINK1 phosphorylates both ubiquitin and the E3 ligase Parkin at Ser65, triggering Parkin recruitment and activation, which in turn ubiquitinates outer mitochondrial membrane proteins and marks damaged mitochondria for autophagic degradation [12]. Consistent with enhanced autophagic activation, TOM70 overexpression significantly increased LC3-II protein levels and decreased p62 while increasing p-Ser65-Ub levels in the T2DM hippocampus. The reduction in p62, a substrate selectively degraded during autophagy, together with the increase in p-Ser65-Ub, a direct product of PINK1 kinase activity, supports activation of the PINK1/Parkin mitophagy pathway, although the LC3-II/LC3-I ratio did not differ among groups. Notably, Kane et al. demonstrated that PINK1 phosphorylates ubiquitin to activate the E3 ubiquitin ligase activity of Parkin [12], and Lazarou et al. established the PINK1-Parkin pathway as the primary mitophagy mechanism in mammalian cells [13], providing the mechanistic framework for our observations. The association between restored TOM70 expression and improved mitochondrial ultrastructure supports the hypothesis that impaired TOM70-dependent mitochondrial protein import represents an upstream event in the cascade of mitochondrial dysfunction in T2DM [21, 22].

Mitochondrial Quality Control and Cognitive Protection

The hippocampus is exquisitely sensitive to mitochondrial dysfunction because of its high metabolic demand and dependence on oxidative phosphorylation for synaptic transmission [23, 24]. Hippocampal mitochondrial dysfunction manifests as impaired ATP production, excessive ROS generation, disrupted calcium homeostasis, and defective mitophagy, all of which converge to compromise synaptic plasticity, a cellular correlate of learning and memory [25–27]. In the present study, T2DM mice exhibited pronounced mitochondrial structural damage. These observations are consistent with previous reports [28]. Importantly, TOM70 overexpression simultaneously restored mitochondrial morphology, decreased oxidative stress, and preserved dendritic spines, suggesting that TOM70-mediated mitochondrial quality control protects synaptic ultrastructure from the deleterious effects of chronic hyperglycemia. Dendritic spines, the postsynaptic sites of excitatory neurotransmission, are highly dynamic structures whose density correlates directly with cognitive function [29, 30]. The preservation of spine density in TOM70-overexpressing T2DM mice provides a structural basis for the behavioral improvements observed in the NORT. Fang et al. reported that mitophagy inhibits amyloid-β and tau pathology and reverses cognitive deficits in AD models, and further demonstrated that defective mitophagy in hippocampal neurons is a key mechanism of AD-related synaptic damage [8]. Kerr et al. reviewed the cellular and molecular mechanisms linking mitophagy to AD [31]. These findings are conceptually aligned with our observations in the T2DM context.

Comparison with AD and T2DM Literature

Our findings extend the current understanding of mitochondrial dysfunction in metabolic cognitive disorders. Previous studies have documented reduced TOM70 expression in the brains of AD patients

[14, 32] and have demonstrated that Aβ peptides can translocate into mitochondria through the TOM/TIM complex [33], suggesting a dual pathogenic role for impaired TOM70 function: deficient mitophagy on one hand and increased mitochondrial Aβ accumulation on the other. The present study is among the first to directly manipulate TOM70 expression in the hippocampus of a T2DM model, establishing a causal link between TOM70 levels and cognitive outcomes. In contrast to the miR-144/FoxO1/AdipoR pathway recently implicated in T2DM cognitive impairment [34], which primarily modulates neuroinflammation and the microglial phenotype, the TOM70-PINK1-Parkin axis represents a cell-intrinsic mitochondrial quality control mechanism that may operate in parallel with, or downstream of, inflammatory signaling. Tyumentsev et al. identified mitochondrial dysfunction as a predictor of processes linked to AD development [35], and Sorrentino et al. demonstrated that enhancing mitophagy protects against cognitive decline [36], further supporting the translational relevance of TOM70 as a therapeutic target. Furthermore, stabilization of MAM function by TOM70, which facilitates proper ER-mitochondrial calcium transfer and phospholipid exchange, may represent an additional mechanism by which TOM70 overexpression preserves neuronal health in T2DM [37]. Future studies employing MAM-specific functional assays are warranted to dissect this aspect of TOM70-mediated neuroprotection.

Limitations and Future Directions

Several limitations of this study should be acknowledged. First, although the increased p-Ser65-Ub levels support activation of PINK1/Parkin-mediated mitophagy, the specific molecular intermediates, including PINK1 stabilization, Parkin translocation, and ubiquitination of mitochondrial substrates, were not directly assessed. Future studies using PINK1- or Parkin-knockout mice in combination with TOM70 overexpression are needed to conclusively establish the mechanistic dependence on this pathway. Second, although the LC3-II/LC3-I ratio, a widely used indicator of autophagic flux, was not significantly altered, the reduction in p62 and the increase in p-Ser65-Ub suggest enhanced autophagic/mitophagic flux; however, autophagic flux was not directly measured. Future studies using autophagy flux inhibitors (e.g., bafilomycin A1 or chloroquine) are warranted. Third, all experiments were conducted exclusively in male mice (n = 10 per group), and cognitive assessments were limited to the NORT and OFT, which precluded sex-specific analyses and comprehensive characterization of cognitive domains such as spatial learning and memory. Future studies should include both sexes and evaluate additional behavioral paradigms. Despite these limitations, our findings identify TOM70 as a promising therapeutic target for T2DM-associated cognitive impairment and provide a foundation for developing TOM70-enhancing strategies, including small-molecule agonists, gene therapy, and pharmacological approaches targeting mitochondrial quality control pathways, for preventing and treating T2DM-related cognitive decline.

Conclusion

In conclusion, this study demonstrates that hippocampal CA1-specific TOM70 overexpression significantly ameliorates cognitive impairment in T2DM mice. The underlying neuroprotective mechanisms involve the restoration of mitochondrial structural integrity, attenuation of mitochondrial

oxidative stress in CA1 neurons, upregulation of LC3-II together with decreased p62 and increased p-Ser65-Ub, a molecular pattern consistent with enhanced PINK1/Parkin-associated mitophagy (direct PINK1 stabilization, Parkin translocation, and autophagic flux were not measured), and preservation of dendritic spine density in the CA1 and CA3 subregions. These findings identify TOM70 as a candidate node linking mitochondrial protein import to cognitive health.

Declarations

Ethics approval

All animal experiments were approved by the Institutional Animal Care and Use Committee of Zhongnan Hospital of Wuhan University (Approval No. ZN2026117) and were conducted in accordance with the Regulations for the Administration of Affairs Concerning Experimental Animals of China.

Consent to participate

Not applicable.

Consent for publication

Not applicable.

Competing interests

The authors declare that they have no known competing financial interests or personal relationships that could have appeared to influence the work reported in this paper.

Funding

This work was supported by the National Natural Science Foundation of China (NO. 82271232).

Author contributions

Wei Zhang: study design and supervision, writing - original draft, writing - review and editing. Jinying Zhao: behavioral testing and daily animal care, tissue collection, histology, and imaging. Xuerui Xiang: data analysis and statistical interpretation. Yuliang Zhou: animal model preparation and surgical procedures, behavioral testing and daily animal care. Shi Cheng: behavioral testing and daily animal care. Zhipeng Xu: review and editing, funding acquisition. All authors have read and agreed to the published version of the manuscript.

Data availability

The datasets generated and analyzed during the current study are available from the corresponding author on reasonable request.

Use of AI-assisted technologies

During the preparation of this work, the authors used ChatGPT (OpenAI) solely to improve the clarity and quality of the language. No generative AI tools were used for data analysis, graphics creation, or interpretation of the results.

Acknowledgements

We are grateful to **Zhang Pei** of the Institutional Center for Shared Technologies and Facilities of Wuhan **Institute of Virology** for **technical support** in transmission electron microscopy.

References

1. Ahmad E, Lim S, Lamptey R, Webb DR, Davies MJ (2022) Type 2 diabetes. Lancet 400(10365):1803–1820
2. Biessels GJ, Despa F (2018) Cognitive decline and dementia in diabetes mellitus: mechanisms and clinical implications. Nat Rev Endocrinol 14(10):591–604
3. Gudala K, Bansal D, Schifano F, Bhansali A (2013) Diabetes mellitus and risk of dementia: a meta-analysis of prospective observational studies. J Diabetes Investig 4(6):640–650
4. Arnold SE, Arvanitakis Z, Macauley-Rambach SL et al (2018) Brain insulin resistance in type 2 diabetes and Alzheimer disease: concepts and conundrums. Nat Rev Neurol 14(3):168–181
5. Hefner M, Baliga V, Amphay K, Ramos D, Hegde V (2021) Cardiometabolic modification of amyloid β in Alzheimer's disease pathology. Front Aging Neurosci 13:721858
6. Sims-Robinson C, Kim B, Rosko A, Feldman EL (2010) How does diabetes accelerate Alzheimer disease pathology? Nat Rev Neurol 6(10):551–559
7. Luo JS, Ning JQ, Chen ZY et al (2022) The role of mitochondrial quality control in cognitive dysfunction in diabetes. Neurochem Res 47(8):2158–2172
8. Fang EF, Hou Y, Palikaras K et al (2019) Mitophagy inhibits amyloid-β and tau pathology and reverses cognitive deficits in models of Alzheimer's disease. Nat Neurosci 22(3):401–412
9. Zappa Villar MF, López Hanotte J, Falomir Lockhart E, Trípodi LS, Morel GR, Reggiani PC (2018) Intracerebroventricular streptozotocin induces impaired Barnes maze spatial memory and reduces astrocyte branching in the CA1 and CA3 hippocampal regions. J Neural Transm (Vienna) 125(12):1787–1803
10. Maruszczak KK, Jung M, Rasool S, Trempe JF, Rapaport D (2022) The role of the individual TOM subunits in the association of PINK1 with depolarized mitochondria. J Mol Med (Berl) 100(5):747–762
11. Matsuda N, Sato S, Shiba K et al (2010) PINK1 stabilized by mitochondrial depolarization recruits Parkin to damaged mitochondria and activates latent Parkin for mitophagy. J Cell Biol 189(2):211–221

12. Kane LA, Lazarou M, Fogel AI et al (2014) PINK1 phosphorylates ubiquitin to activate Parkin E3 ubiquitin ligase activity. J Cell Biol 205(2):143–153
13. Lazarou M, Sliter DA, Kane LA et al (2015) The ubiquitin kinase PINK1 recruits autophagy receptors to induce mitophagy. Nature 524(7565):309–314
14. Cao X, Chen Y, Sang X et al (2022) Impact prediction of translocation of the mitochondrial outer membrane 70 as biomarker in Alzheimer's disease. Front Aging Neurosci 14:1013943
15. Devi L, Prabhu BM, Galati DF, Avadhani NG, Anandatheerthavarada HK (2006) Accumulation of amyloid precursor protein in the mitochondrial import channels of human Alzheimer's disease brain is associated with mitochondrial dysfunction. J Neurosci 26(35):9057–9068
16. Lu Z, Jia Q, Wang R et al (2011) Hypoglycemic activities of A- and B-type procyanidin oligomer-rich extracts from different cinnamon barks. Phytomedicine 18(4):298–302
17. Zhang J, Qiu H, Huang J et al (2018) Establishment of a diabetic myocardial hypertrophy model in Mus musculus castaneus mouse. Int J Exp Pathol 99(6):295–303
18. Adaikkan C, Joseph J, Foustoukos G et al (2024) Silencing CA1 pyramidal cells output reveals the role of feedback inhibition in hippocampal oscillations. Nat Commun 15(1):2190
19. Araiso Y, Imai K, Endo T (2022) Role of the TOM complex in protein import into mitochondria: structural views. Annu Rev Biochem 91:679–703
20. Jin SM, Lazarou M, Wang C, Kane LA, Narendra DP, Youle RJ (2010) Mitochondrial membrane potential regulates PINK1 import and proteolytic destabilization by PARL. J Cell Biol 191(5):933–942
21. Narendra DP, Youle RJ (2024) The role of PINK1-Parkin in mitochondrial quality control. Nat Cell Biol 26(10):1639–1651
22. Wang P, Wang D, Yang Y et al (2020) Tom70 protects against diabetic cardiomyopathy through its antioxidant and antiapoptotic properties. Hypertens Res 43(10):1047–1056
23. Li S, Sheng ZH (2022) Energy matters: presynaptic metabolism and the maintenance of synaptic transmission. Nat Rev Neurosci 23(1):4–22
24. Olesen MA, Torres AK, Jara C et al (2020) Premature synaptic mitochondrial dysfunction in the hippocampus during aging contributes to memory loss. Redox Biol 34:101558
25. Cicali KA, Torres AK, Tapia-Rojas C (2026) Synaptic mitochondria in aging and neurodegenerative diseases: functional decline and vulnerability. Neural Regen Res 21(6):2145–2152
26. Sayehmiri F, Motamedi F, Batool Z et al (2024) Mitochondrial plasticity and synaptic plasticity crosstalk; in health and Alzheimer's disease. CNS Neurosci Ther 30(8):e14897
27. Todorova V, Blokland A (2017) Mitochondria and synaptic plasticity in the mature and aging nervous system. Curr Neuropharmacol 15(1):166–173
28. Lu LL, Liu LZ, Li L et al (2024) Sodium butyrate improves cognitive dysfunction in high-fat diet/streptozotocin-induced type 2 diabetic mice by ameliorating hippocampal mitochondrial damage through regulating AMPK/PGC-1α pathway. Neuropharmacology 261:110139

29. Choi JE, Kaang BK (2024) Plasticity of dendritic spines underlies fear memory. Neuroscientist 30(6):690–703
30. Runge K, Cardoso C, de Chevigny A (2020) Dendritic spine plasticity: function and mechanisms. Front Synaptic Neurosci 12:36
31. Kerr JS, Adriaanse BA, Greig NH et al (2017) Mitophagy and Alzheimer's disease: cellular and molecular mechanisms. Trends Neurosci 40(3):151–166
32. Chai YL, Xing H, Chong JR et al (2018) Mitochondrial translocase of the outer membrane alterations may underlie dysfunctional oxidative phosphorylation in Alzheimer's disease. J Alzheimers Dis 61(2):793–801
33. Hansson Petersen CA, Alikhani N, Behbahani H et al (2008) The amyloid β-peptide is imported into mitochondria via the TOM import machinery and localized to mitochondrial cristae. Proc Natl Acad Sci U S A 105(35):13145–13150
34. Zhao J, Zhou Y, Cheng S, Shen J, Li Y, Xu Z (2026) MiR-144 regulates cognitive dysfunction via NLRP3 inflammasome and FoxO1/AdipoR pathway in T2DM mice. Mol Neurobiol. https://doi.org/10.1007/s12035-026-05897-7
35. Tyumentsev MA, Stefanova NA, Muraleva NA et al (2018) Mitochondrial dysfunction as a predictor and driver of Alzheimer's disease-like pathology in OXYS rats. J Alzheimers Dis 63(3):1075–1088
36. Sorrentino V, Romani M, Mouchiroud L et al (2017) Enhancing mitochondrial proteostasis reduces amyloid-β proteotoxicity. Nature 552(7684):187–193
37. Filadi R, Leal NS, Schreiner B et al (2018) TOM70 sustains cell bioenergetics by promoting IP3R3-mediated ER to mitochondria Ca^{2+} transfer. Curr Biol 28(3):369–82e6

Figures

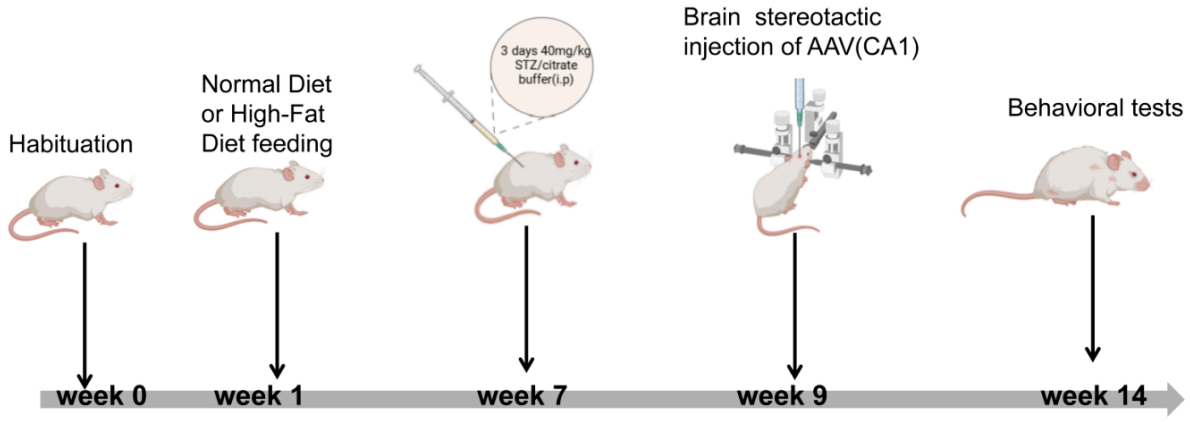


Figure 1

Experimental timeline and grouping. Adult male C57BL/6J mice were randomized into four groups (n = 10/group): Control, Control + AAV-TOM70, T2DM, and T2DM + AAV-TOM70. T2DM was induced by high-fat diet (HFD) feeding for 6 weeks followed by low-dose streptozotocin (STZ, 40 mg/kg, i.p., daily for 3 consecutive days). Bilateral stereotactic injection of AAV-Tomm70a-2A-EGFP or AAV-empty control into the hippocampal CA1 region was performed at week 9. Behavioral assessments (open field test and novel object recognition test) were conducted 4 weeks post-injection (week 14).

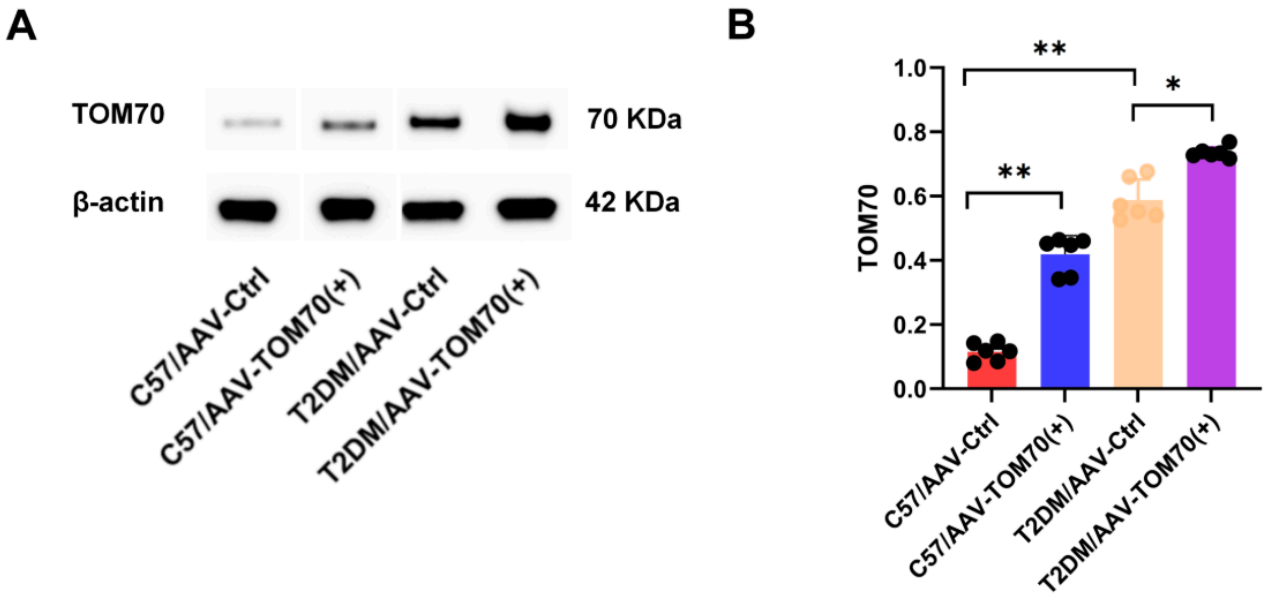


Figure 2

Hippocampal CA1 AAV-mediated TOM70 overexpression validation. (A) Representative Western blot images showing TOM70 protein expression in hippocampal CA1 tissues from the four experimental groups. β-actin (42 kDa) was used as the loading control. TOM70 was detected at the expected molecular weight (~70 kDa). (B) Quantitative densitometric analysis of TOM70 protein levels normalized to β-actin. Data are expressed as mean ± SEM (n = 6 mice/group). AAV-TOM70 significantly increased TOM70 expression in both C57BL/6J and T2DM mice compared with control groups (*P < 0.05, **P < 0.01, one-way ANOVA followed by Tukey's post hoc test).

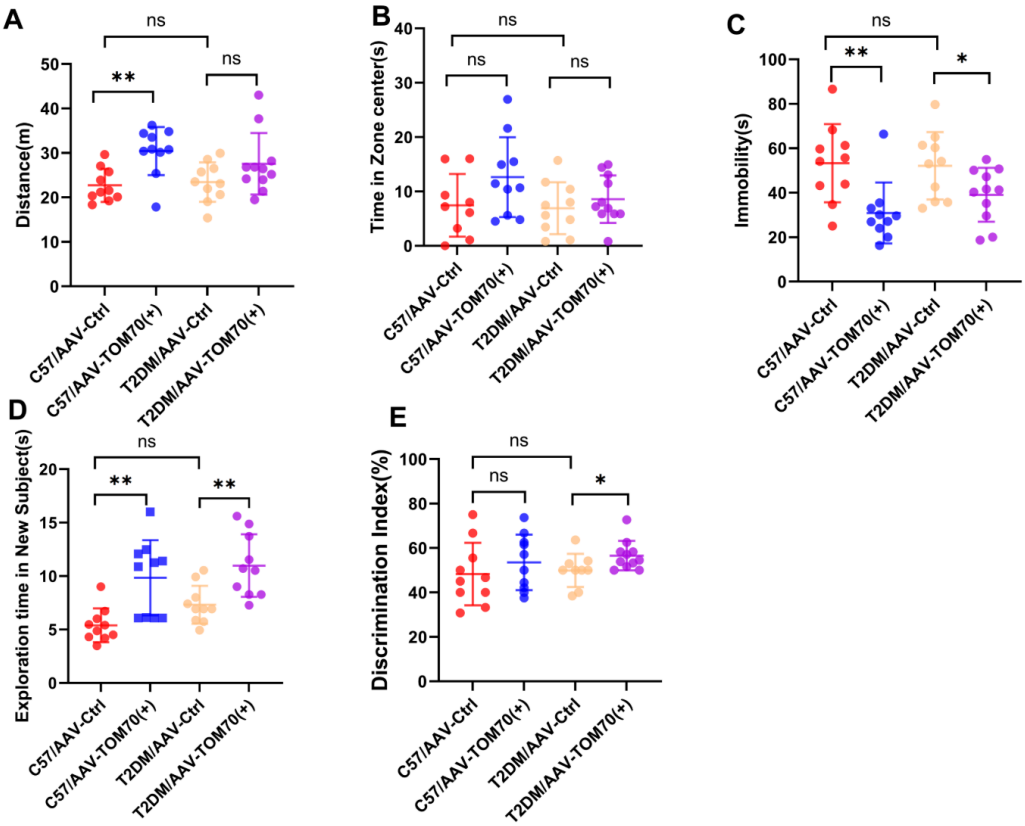


Figure 3

TOM70 overexpression ameliorates behavioral deficits in T2DM mice. (A) Total distance traveled in the open field test. (B) Time spent in the center zone of the open field test. (C) Immobility time of the open field test. (D) Exploration time for the familiar object and novel object of the novel object recognition test (NORT). (E) Discrimination index calculated as (Tnovel - Tfamiliar) / (Tnovel + Tfamiliar) of the NORT. Data are presented as mean ± SEM (n = 10). *P < 0.05, **P < 0.01, ***P < 0.001.

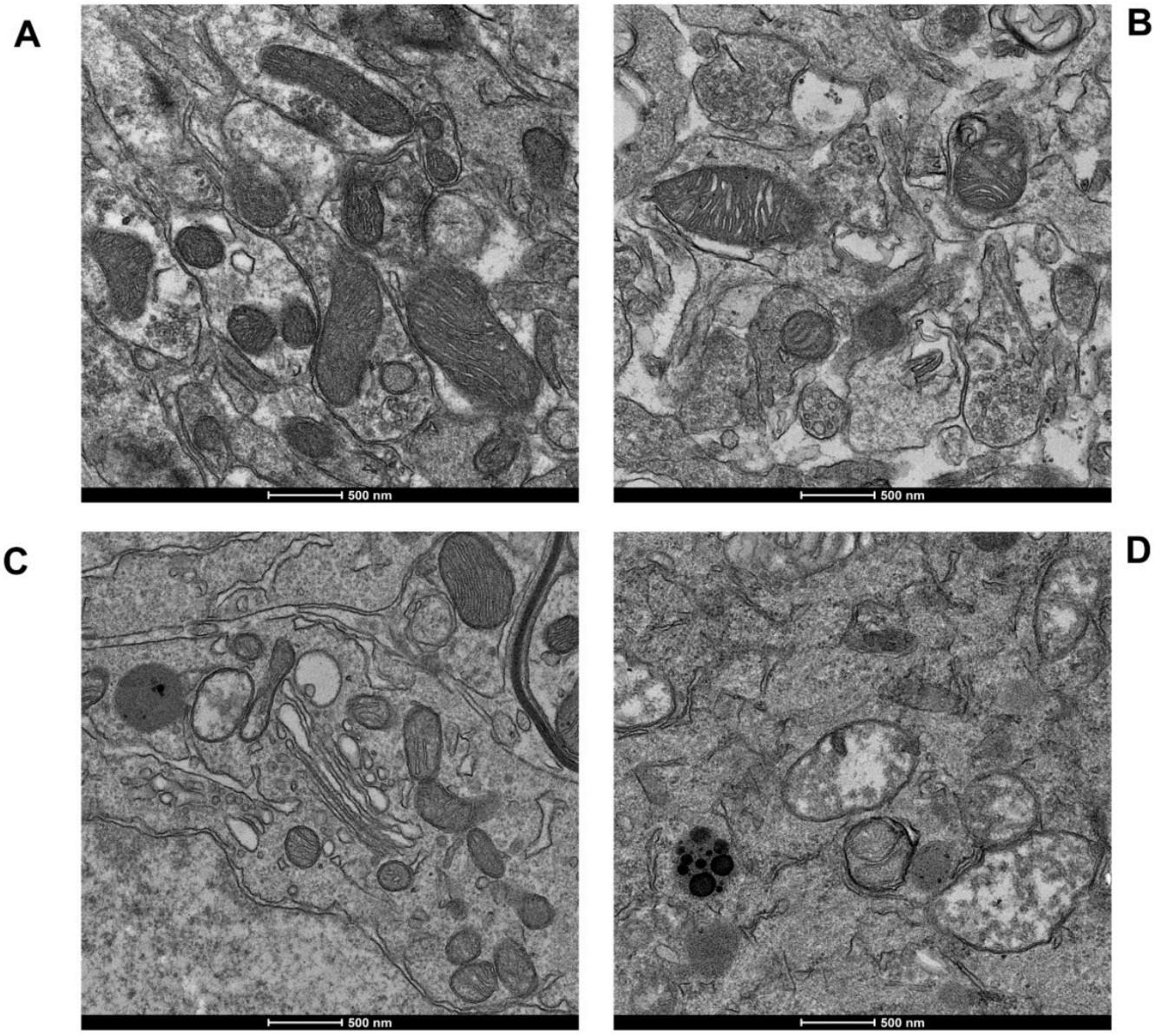


Figure 4

Transmission electron microscopy (TEM) of hippocampal neuron mitochondria. (A) C57/AAV-Ctrl: normal mitochondrial ultrastructure with intact cristae. (B) C57/AAV-TOM70(+): mitochondria with preserved morphology after TOM70 overexpression. (C) T2DM/AAV-Ctrl: swollen mitochondria with disrupted cristae and reduced matrix density. (D) T2DM/AAV-TOM70(+): partial restoration of mitochondrial morphology. Scale bars = 500 nm.

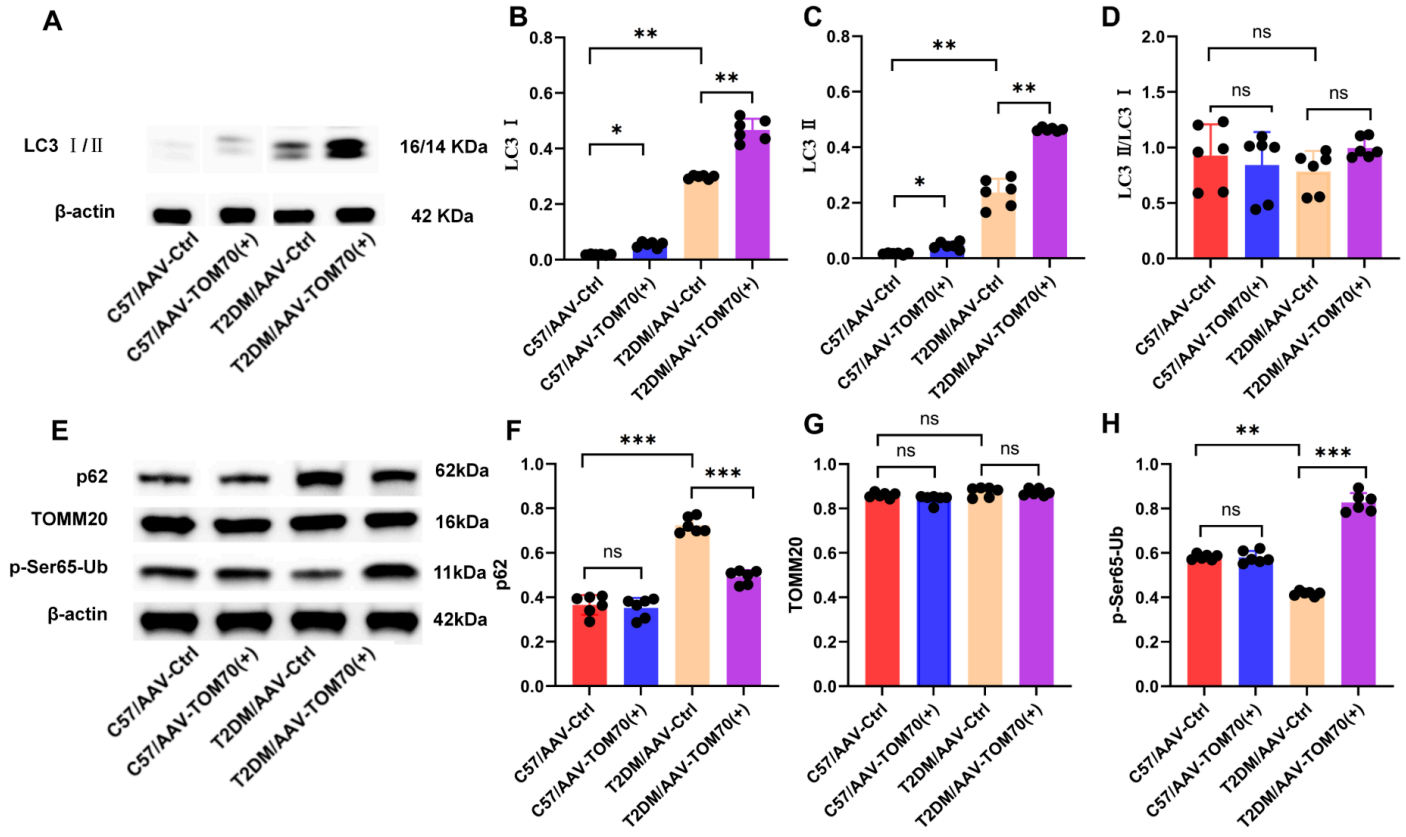


Figure 5

TOM70 overexpression modulates LC3 and mitophagy-related protein expression in the hippocampus. (A) Representative Western blot images showing LC3-I (16 kDa) and LC3-II (14 kDa) protein bands in hippocampal tissues from the four experimental groups. β-actin (42 kDa) was used as the loading control. Full-length blots are presented in Supplementary Material. (B) Densitometric quantification of LC3-I expression normalized to β-actin. TOM70 overexpression modestly increased LC3-I levels in both C57BL/6J and T2DM mice compared with their respective AAV-ctrl groups (*P < 0.05 in C57 mice; **P < 0.01 in T2DM mice vs. T2DM/AAV-Ctrl). (C) Densitometric quantification of LC3-II expression normalized to β-actin. TOM70 overexpression markedly increased LC3-II levels in both groups (**P < 0.01 vs. respective AAV-Ctrl), with a more pronounced effect in the T2DM group. (D) Quantification of the LC3-II/LC3-I ratio across groups (ns, P > 0.05). (E) Representative Western blot images showing p62 (62 kDa), TOMM20 (16 kDa), and p-Ser65-Ub (11 kDa) protein bands in hippocampal tissues from the four experimental groups. β-actin (42 kDa) was used as the loading control. (F) Densitometric quantification of p62 expression normalized to β-actin. T2DM/AAV-Ctrl mice exhibited significantly higher p62 levels than C57/AAV-Ctrl mice, and TOM70 overexpression significantly reduced p62 levels in T2DM mice (***P < 0.001). (G) Densitometric quantification of TOMM20 expression normalized to β-actin (ns, P > 0.05). (H) Densitometric quantification of p-Ser65-Ub expression normalized to β-actin. T2DM/AAV-Ctrl mice exhibited significantly lower p-Ser65-Ub levels than C57/AAV-Ctrl mice (**P < 0.01), and TOM70 overexpression significantly increased p-Ser65-Ub levels in T2DM mice (***P < 0.001). Data are presented as mean ± SEM (n = 6 mice/group). *P < 0.05, **P < 0.01, ***P < 0.001; ns, not significant.

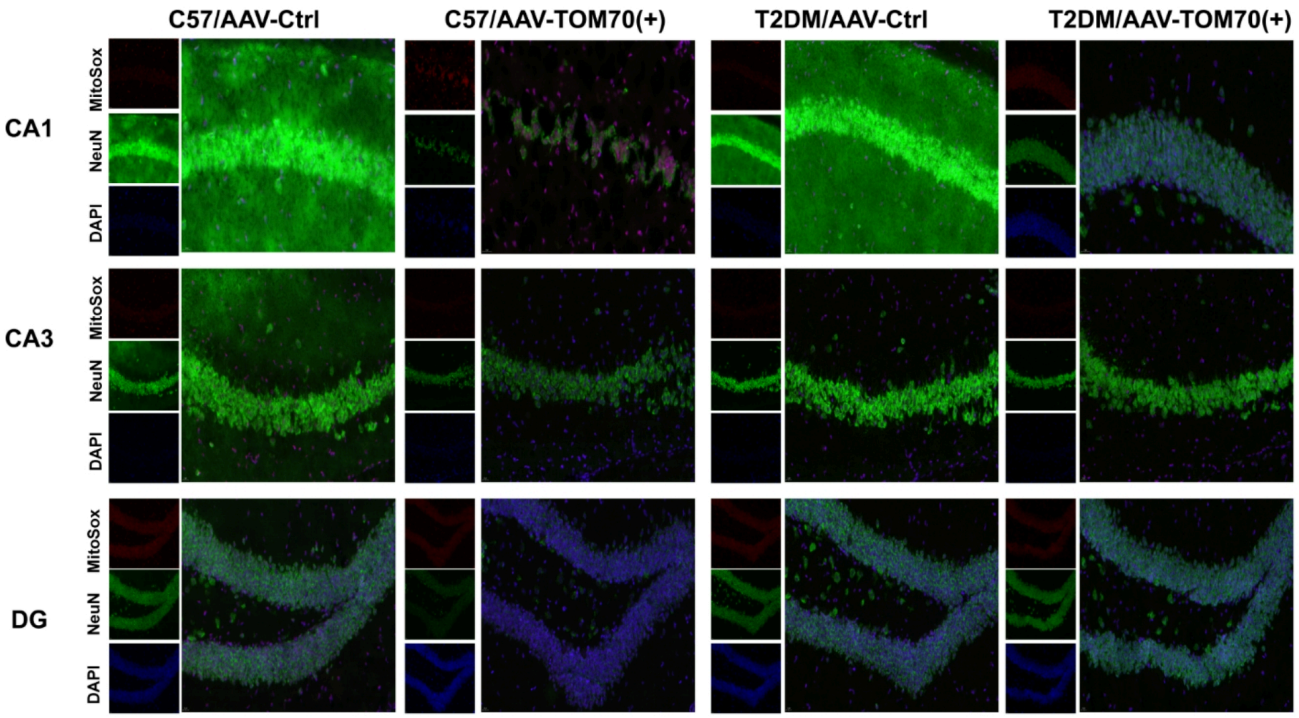


Figure 6

Representative confocal immunofluorescence images showing mitochondrial superoxide production (MitoSOX Red), mature neurons (NeuN, green), and nuclear staining (DAPI, blue) in the hippocampal CA1, CA3, and DG subregions of the four experimental groups (C57/AAV-Ctrl, C57/AAV-TOM70(+), T2DM/AAV-Ctrl, and T2DM/AAV-TOM70(+)). For each subregion, three individual fluorescence channels (MitoSOX, NeuN, DAPI) are shown alongside a merged image (right-most panel of each group). Scale bars = 20 μm.

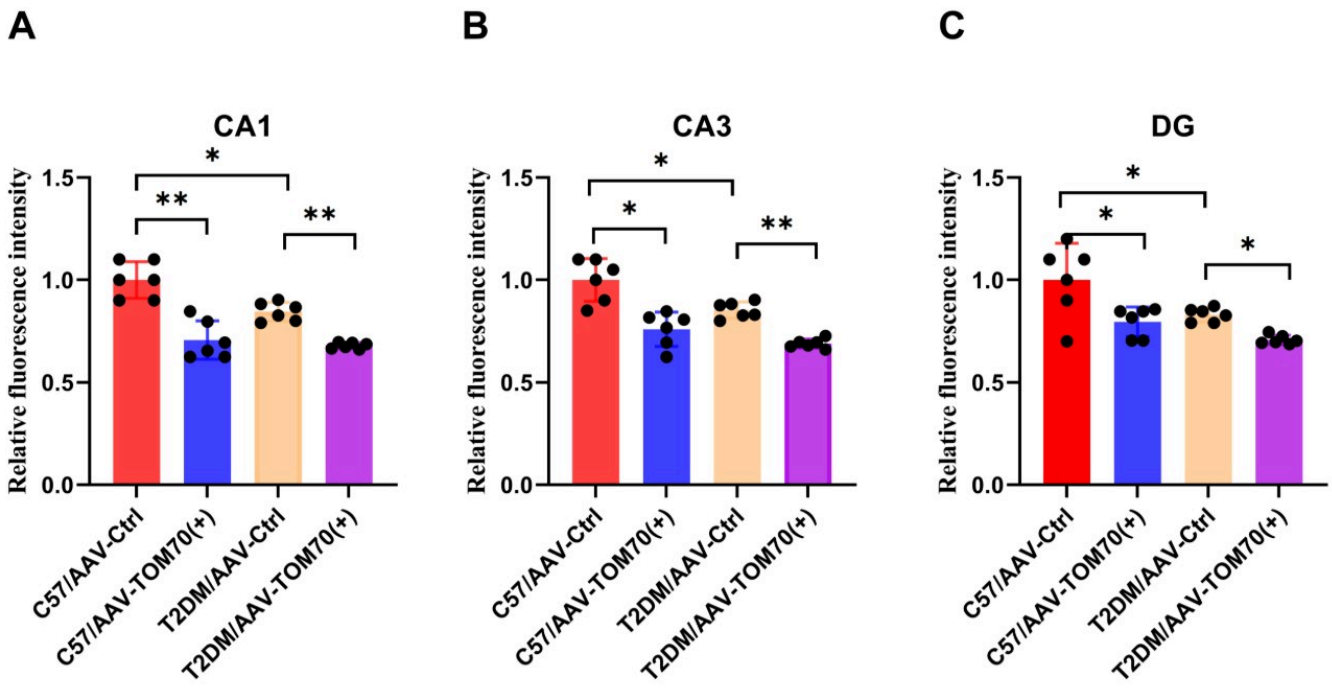


Figure 7

TOM70 overexpression attenuates mitochondrial oxidative stress in hippocampal neurons across CA1, CA3, and DG subregions. (A) Quantitative analysis of CA1 MitoSOX relative fluorescence intensity. (B) Quantitative analysis of CA3 MitoSOX relative fluorescence intensity. (C) Quantitative analysis of DG MitoSOX relative fluorescence intensity. Data are presented as mean ± SEM (n = 6 mice/group). *P < 0.05, **P < 0.01; ns, not significant.

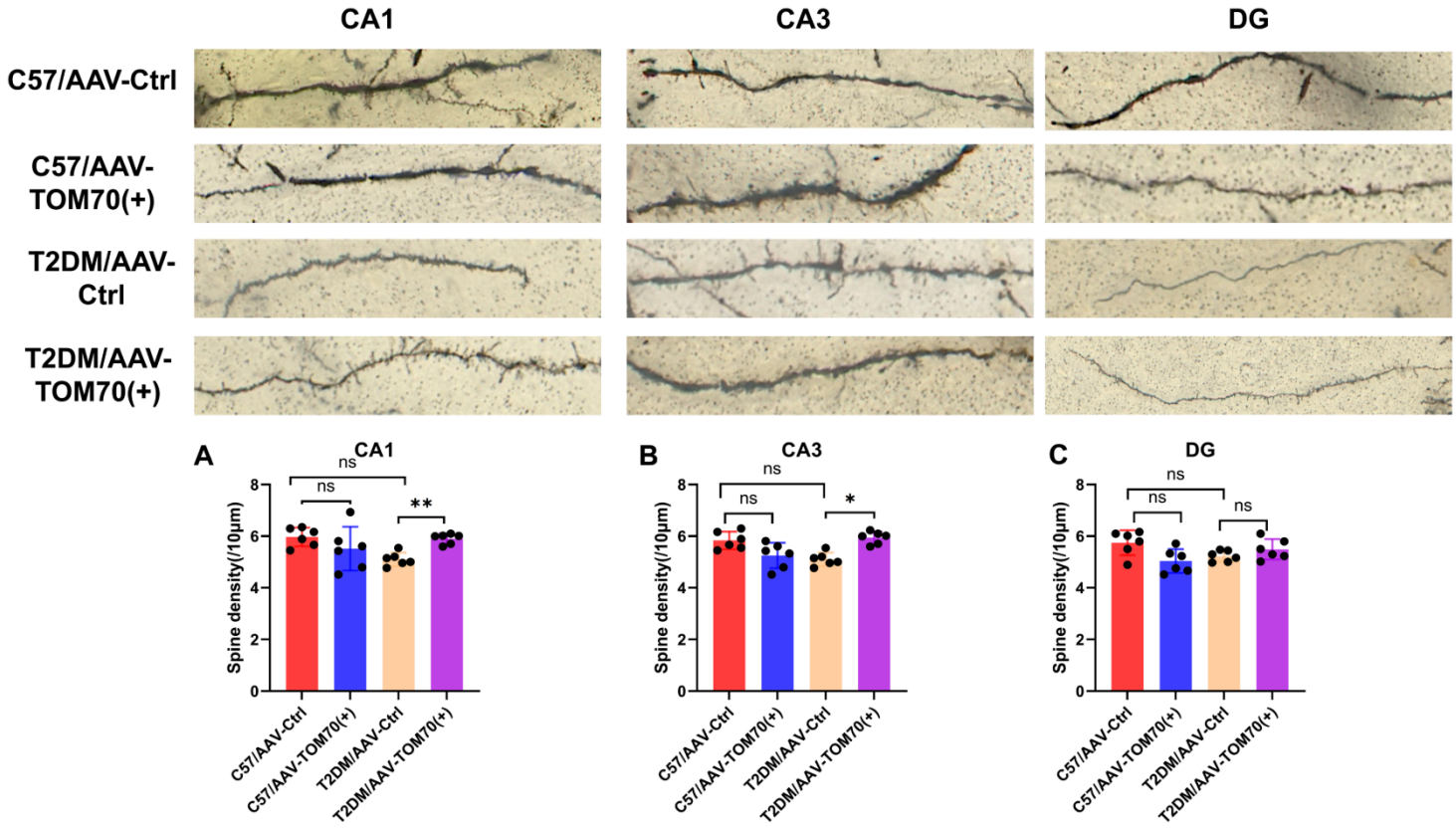


Figure 8

Effect of TOM70 overexpression on dendritic spine density in hippocampal CA1, CA3, and DG neurons. Upper panels: representative photomicrographs. Golgi-stained dendritic segments from CA1 pyramidal neurons (left column), CA3 pyramidal neurons (middle column), and DG granule cells (right column) across the four experimental groups (rows). Scale bars = 10 μm. Lower panels: quantitative analysis of dendritic spine density (spines/10 μm dendrite length). (A) CA1 region. Spine density was comparable between C57/AAV-Ctrl and T2DM/AAV-Ctrl mice (ns). TOM70 overexpression in T2DM mice (T2DM/AAV-TOM70(+)) significantly increased spine density relative to T2DM/AAV-Ctrl (**P < 0.01). C57/AAV-TOM70(+) showed a non-significant trend toward reduced spine density compared with C57/AAV-Ctrl (ns). (B) CA3 region. Similar pattern: no significant difference between C57/AAV-Ctrl and T2DM/AAV-Ctrl (ns). TOM70 overexpression significantly increased spine density in T2DM/AAV-TOM70(+) compared with T2DM/AAV-Ctrl (*P < 0.05). (C) DG region. No significant differences were observed across all four groups. Data are presented as mean ± SEM (n = 6 mice/group). *P < 0.05, **P < 0.01; ns, not significant.

Supplementary Files

This is a list of supplementary files associated with this preprint. Click to download.

- WB.zip